Journal of Molecular Liquids 356 (2022) 118957

Contents lists available at ScienceDirect

Journal of Molecular Liquids

journal homepage: www.elsevier.com/locate/molliq

Zirconium-organic framework as a novel adsorbent for arsenate remediation from aqueous solutions

Roxana Paz [a], Herlys Viltres [b,*], Nishesh Kumar Gupta [c,d], Kaptan Rajput [e], Debesh R. Roy [e], Adolfo Romero-Galarza [f], Mark C. Biesinger [g], Carolina Leyva [a,*]

[a] Instituto Politécnico Nacional, Centro de Investigación en Ciencia Aplicada y Tecnología Avanzada, CDMX, Mexico
[b] School of Engineering Practice and Technology, McMaster University, 1280 Main Street West Hamilton, Ontario L8S 4L8, Canada
[c] University of Science and Technology (UST), Daejeon, Republic of Korea
[d] Department of Land, Water, and Environment Research, Korea Institute of Civil Engineering and Building Technology (KICT), Goyang, Republic of Korea
[e] Materials and Biophysics Group, Department of Applied Physics, S. V. National Institute of Technology, Surat, India
[f] Department of Chemical Engineering, School of Chemistry, Universidad Autónoma de Coahuila, Mexico
[g] Surface Science Western, Western University, Ontario, Canada

ARTICLE INFO

Article history:
Received 31 July 2021
Revised 13 March 2022
Accepted 16 March 2022
Available online 19 March 2022

Keywords:
Adsorption
Arsenate
DFT calculations
Spectroscopy
Zr-MOF

ABSTRACT

The removal of arsenic species in water is a global challenge due to its high toxicity and carcinogenicity. In this work, a stable zirconium metal-organic framework (Zr-MOF) has been synthesized for As(V) removal. The Zr-MOF adsorbed As(V) effectively in the pH range of 4–9 with the maximum adsorption capacity of 278 mg g^{-1}. The experimental data modelling suggested a spontaneous adsorption process involving physicochemical forces. The spectroscopic analysis confirmed the binding of As(V) on the Zr-sites via a ligand-exchange mechanism involving Zr—OH. Another possible mechanism was the interaction of As(V) with the dissociation of Zr—O(linker) sites. These mechanisms were further confirmed by theoretical calculations, where the Zr—(μ_3-O) bridges (binding energy ~4.38 eV) bind As(V) more strongly than the Zr—O—C linkages (binding energy ~4.11 eV). The material regeneration was successfully carried out with HCl solution, where the regeneration efficacy remained ~90% for five cycles. Thus, the study provided a detailed investigation on the As(V) adsorption over Zr-MOF.

1. Introduction

Water contamination with arsenic (As) is a global challenge due to its high toxicity [1]. Arsenic in the environment results from several natural and anthropogenic activities, including geochemical reactions, microbial activity, industrial mining, combustion of fossil fuels, and pesticides [2]. Arsenic is considered a carcinogenic pollutant; exposure to it could cause skin, liver, kidney, and bladder cancer [3]. For this reason, the World Health Organization has categorized it as one of the principal issues amongst toxic substances [4]. The most predominating As species in the surface water is arsenate (As(V)) [5]. As(V) ions have high mobility in water systems, which leads to large accumulation into the living beings through the food chain. Effective removal of As(V) ions in water bodies is imperative [6].

Different treatment technologies like chemical precipitation [7], reverse osmosis [8], ion exchange [9], electro-coagulation [10], adsorption [11,12], and bioremediation [13] have been studied for the removal of arsenic species from wastewater. Among these methods, adsorption is the most studied technique due to its ease of operation, simplicity, affordability, and high removal efficiency [14]. Metal-organic frameworks (MOFs) are a sub-class of inorganic-organic hybrid materials, which have gained recent fame due to their large surface area and porosity. The physicochemical properties of MOFs could be tuned by choosing appropriate metal (ions/cluster) nodes and organic ligands as linkers. These structural and functional flexibilities have been adopted in various task-specific applications in the domain of energy and the environment. These materials are good candidates for wastewater treatments due to their high surface area, adsorption capacity, chemical functionalities, specific host-guest interactions, and chemical stability [15,16].

Zirconium(IV)-based MOFs are known to possess high adsorption capacity for arsenate species [17,18], which is due to strong Lewis acid-base interactions between As(V) ions and Zr—OH groups [19]. UiO-66 (Zr-terephthalate MOF) is the most explored Zr-based MOF for As(V) adsorption process [20–23], with the max-

* Corresponding authors.
E-mail addresses: viltresh@mcmaster.ca (H. Viltres), zleyva@ipn.mx (C. Leyva).

https://doi.org/10.1016/j.molliq.2022.118957
0167-7322/

imum adsorption capacity of 303.0 mg g^{-1} reported by Wang *et al* [24]. Subbaiah *et al* reported the maximum As(V) adsorption capacity of 230.3 mg g^{-1} over a modulator (benzoic acid)-driven Zr-fumaric acid MOF [25]. Among Zr-MOFs, MOF-808 (Zr-trimesate MOF) is another possible candidate, which could be used for the As(V) removal. Li and coworkers reported MOF-808 for As (V) removal with the maximum capacity of 24.8 mg g^{-1} [26]. Though the study pointed out MOF-808 application in As(V), it lacked vital information on parameter optimization and adsorption mechanism. Besides, many reported studies on As(V) adsorption over Zr-MOFs lack spectroscopic evidence for the proposed adsorption mechanism.

In this study, we have reported As(V) adsorption over Zr-based MOF (MOF-808). The structural and functional characteristics of Zr-MOF were studied by various analytical techniques. We have explored the As(V) adsorption mechanism through experimental and spectroscopic results. Moreover, the preferential As(V) binding sites in the Zr-MOF have been identified through density functional theory (DFT) calculations. The reusability of the adsorbent was evaluated for multiple cycles, and the adsorbent stability was confirmed through powder X-ray diffraction (PXRD) and Fourier-Transform infrared (FTIR) spectroscopy. The study confirmed Zr-MOF as a stable MOF with a high As(V) removal capacity.

2. Materials and methods

2.1. Chemicals and reagents

Sodium arsenate dibasic heptahydrate ($Na_2HAsO_4{\cdot}7H_2O$, ACS reagent ≥98%), zirconyl chloride octahydrate ($ZrOCl_2{\cdot}8H_2O$, reagent grade 98%), trimesic acid (H_3BTC, purity 95%), anhydrous dimethylformamide (DMF, purity 99.8%), sodium hydroxide pellets (NaOH, purity ≥97.0%), hydrochloric acid (HCl ACS reagent, 37%), ICP standards of As(V), Cd(II), Pb(II), Fe(III), Mg(II), Ca(II) cations (1000 ± 2 mg L^{-1}) were supplied by Sigma-Aldrich, Germany. Methanol (ACS reagent chemical, anhydrous, 99.8%) was purchased from Baker®. The reagents were used without further purification.

2.2. Zr-MOF synthesis

A 2.57 g of $ZrOCl_2{\cdot}8H_2O$ and 1.68 g of trimesic acid (H_3BTC) were dissolved in 40 mL of DMF by magnetic stirring and sonication. The solution was heated in an oven at 180 °C for 24 h. The supernatant solid was separated by centrifugation and washed three times with DMF and methanol. The final product (Zr-MOF) was dried at 50 °C for 24 h.

2.3. Analytical instruments

The detailed information on the instrumental techniques is available in **Section S1**.

2.4. Adsorption studies

The adsorption studies were conducted at room temperature by soaking 30 mg of the MOF in a 30 mL As(V) ion solution (100 mg L^{-1}) for 12 h at pH 7. The conditions were changed accordingly to understand the effect of experimental parameters on the As(V) adsorption capacity of the MOF. The solution pH was adjusted using $NaOH/HNO_3$ solutions (0.1 mol L^{-1}). The pH measurement was conducted on a Thermo Scientific pH meter. The regeneration of the As-loaded composite was done using a 0.1 mol L^{-1} NaOH/HCl aqueous solution. The adsorption capacity (q_e, mg g^{-1}) at equilibrium was calculated using **Eq. (1)**.

$$q_e = \frac{(C_0 - C_e) * V}{m} \quad (1)$$

where V, m, C_0, and C_e are the volume of aqueous solution (L), amount of the adsorbent (g), initial concentration (mg L^{-1}), and equilibrium concentration (mg L^{-1}), respectively.

The breakthrough study was conducted in a narrow glass column with 0.04 g of the MOF packed with glass wool. A multi-element solution containing 5.0 mg L^{-1} each of As(V), Cd(II), Fe (III), Pb(II), Ca(II), and Mg(II) at pH 7 was passed through the adsorbent bed at a fixed flow rate of 0.5 mL min^{-1}. The effluent As(V) concentration was measured every 5 min. The breakthrough and exhaustive capacity of As(V) were calculated using **Eq. (2)**.

$$q = \frac{C_0 Q}{m} \int_0^{t_b} (1 - \frac{C}{C_0}) dt \quad (2)$$

where C_0–initial concentration (5.0 mg L^{-1}), Q–flow rate (0.5 mL min^{-1}), m–the mass of MOF (0.04 g), and t_b–breakthrough time.

2.5. Computational protocol

Information on DFT calculations is available in **Section S2**.

3. Results and discussion

3.1. Zr-MOF characterization

The FTIR spectra of Zr-MOF and H_3BTC linker are shown in Fig. 1**b**. In the FTIR spectrum of H_3BTC, bands at 1704, 1606, and 1452 cm^{-1} are related to the stretching vibrations of C═O and C═C in the linker. Whereas the broadband at 3600–2600 cm^{-1} covers distinct bands for —COOH and C—H stretching [29]. In the FTIR spectrum of Zr-MOF, the broadband for —COOH disappeared, and the band at 1704 cm^{-1} shifted. The broadband around 3400 cm^{-1} was assigned to the O—H stretching vibrations in Zr—OH and adsorbed water molecules. The band at 1656, 1617, and 1387 cm^{-1} were assigned to the various stretching modes of Zr-carboxylate bonds. The C═C stretching vibrations of the aromatic skeleton are attributed to the band at 1441 cm^{-1} [30]. Bands in the 1200–800 cm^{-1} range were attributed to the C—H bending modes, respectively [30]. The bands observed at 711 and 657 cm^{-1} were due to the asymmetric vibrations of the Zr—(μ_3-O) bridges in the MOF's structural framework. The band at 460 cm^{-1} corresponded to the stretching vibrations of Zr—O(carboxylate) bonds [31]. Thus, the H_3BTC linkers chemically coordinated with the Zr ions in the MOF.

The Raman spectrum of Zr-MOF is shown in Fig. 1**c**. The peak at 415 cm^{-1} was assigned to the Zr—O—C (carboxylate) stretching modes. The peaks at 806 and 866 cm^{-1} were attributed to the C—H bending mode, and the high-intensity peak at 1002 cm^{-1} was associated with the stretching vibrations of C═C (aromatic ring). The asymmetric and symmetric stretching modes of carboxylate bridges were observed at 1587 and 1469 cm^{-1}, respectively [32,33].

The thermogravimetric analysis (TGA) profile of Zr-MOF was generated in the temperature range of 30–600 °C (Fig. 1**d**). In the TGA profile, three main mass loss stages were observed in the studied range. The first mass loss was recorded in the 30–110 °C range for the evaporation of physically adsorbed water molecules., which accounted for the ~8% of mass loss. The mass loss in the second stage (110–400 °C) was associated with the removal of chemically bonded water molecules and physically adsorbed solvent (DMF/methanol) molecules. The thermal degradation of MOF started after 400 °C, which was considered the third stage of mass loss [34,35]. Thus, MOF was thermally stable up to 400 °C.

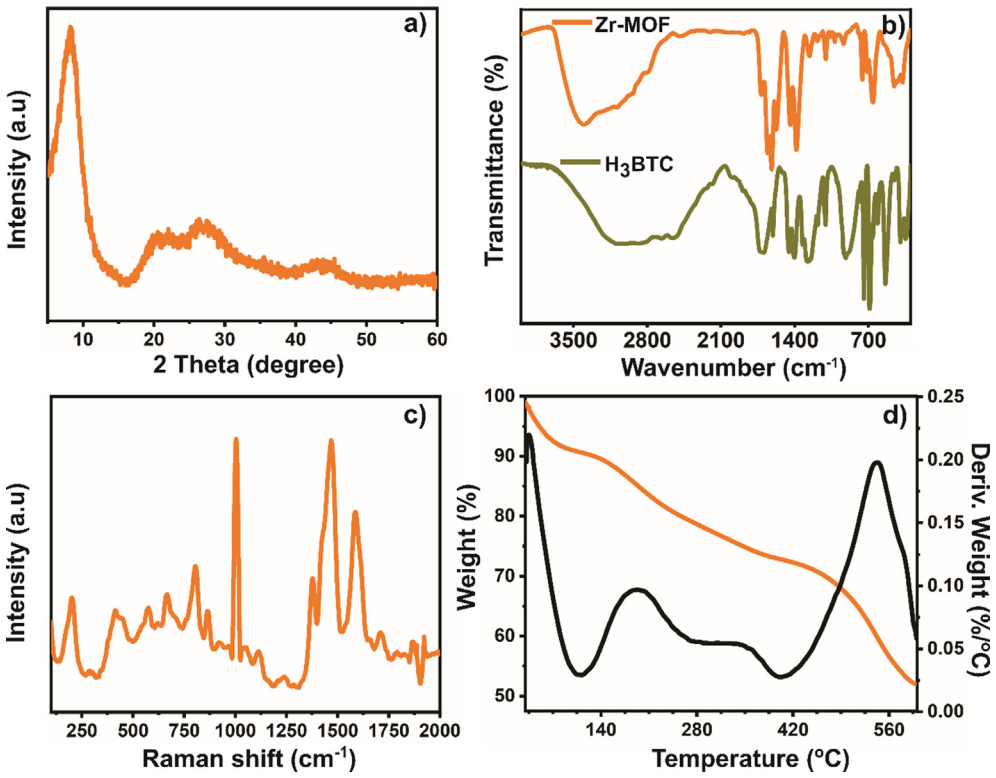

Fig. 1. (**a**) PXRD patterns, (**b**) FTIR, (**c**) Raman spectra, and (**d**) TGA profile of Zr-MOF. The PXRD pattern of Zr-MOF is shown in Fig. 1**a**. The pattern has a high-intensity broad peak in the 5-15° range with the maxima at 8.2°. The reported zirconium trimesate MOF (MOF-808) has peaks at 2θ = 8.32° and 8.69° (**Fig. S1**) [27]. The broadening of the diffraction peaks was due to the low crystallinity of the MOF formed due to the use of $ZrOCl_2{\cdot}8H_2O$ as Zr precursor. Ardila-Suárez *et al* used different Zr precursors for the fabrication of MOF-808, and the sample synthesized using $ZrOCl_2{\cdot}8H_2O$ precursor showed the lowest crystallinity [28].

The X-ray photoelectron spectroscopy (XPS) full scan of Zr salt, H_3BTC, and Zr-MOF are shown in Fig. 2**a**. The Zr-MOF has peaks for Zr 3d, Cl 2p, C 1 s, and O 1 s at their respective binding energy. The small presence of Cl (1.2%) was due to the residual chloride ions from the Zr-salt precursor (**Table S1**). The high-resolution XPS (HRXPS) C 1 s spectrum of Zr-MOF has four contributions at 284.7, 286.0, 288.6, and 290.8 eV, which were assigned to the C═C (aromatic), C—O, O—C═O, and satellite, respectively (Fig. 2**b**, **Table S2**) [36,37]. The HRXPS O 1 s spectrum of Zr-MOF deconvoluted into three peaks at 530.1, 531.6, and 532.7 eV corresponding to the Zr—O—Zr, Zr—O—C, and Zr—OH, respectively (Fig. 2**c**, **Table S3**) [21]. The HRXPS Zr 3d spectrum has two peaks at 182.7 (Zr $3d_{5/2}$) and 185.1 eV (Zr $3d_{3/2}$) for Zr_6 clusters in Zr-MOF (Fig. 2**d**) [37]. The Zr $3d_{5/2}$ peak at 183.2 eV for Zr-salt shifted to 182.7 eV in Zr-MOF due to a change in the electron density on Zr of Zr-MOF (**Table S4**).

3.2. Zr-MOF stability

The acid/base stability of a MOF is one of the important aspects of its application in wastewater treatment [38]. In the present study, the Zr-MOF stability was evaluated in the pH range of 4–9 (same range adopted for pH-dependent study) using FTIR and PXRD (Fig. 3). In the FTIR spectra, the band corresponding to O—H bonds broadened along with the increase in intensity due to the adsorbed water molecules. The bands in the range of 1700–1300 cm^{-1} (carboxylate stretching) and 700–400 cm^{-1} (Zr—O) fully overlapped with that of the synthesized MOF (Fig. 3**a**). Moreover, the PXRD patterns of MOF remain unaltered in the entire pH range with no evolution of peaks for ZrO_2 (Fig. 3**b**) [39]. Thus, it was confirmed that the Zr-MOF was highly stable in the studied pH range.

3.3. Effect of parameters

The effect of adsorbent dosage was studied in the 5–70 mg range without changing other parameters (Fig. 4**a**). The adsorption capacity increased with the increasing dosage from 5 to 10 mg, which was followed by a consistent drop beyond 10 mg. With the increasing dosage, the number of adsorption sites increases for the As(V) ions, which improves the adsorption capacity. But, after a specific dosage (the equilibrium dosage), the increasing adsorption sites become less relevant as the % adsorption efficiency increases slightly, but the adsorption capacity decreases to a larger extent [40].

The effect of As(V) concentration was studied in the 5–350 ppm range (Fig. 4**b**). The adsorption capacity increased linearly with the increasing concentration and reached a maximum of 278 mg g^{-1} (77% removal) for an initial concentration of 350 ppm. The increasing concentration of As(V) ions for a limited number of adsorption sites increased the As(V) concentration gradient near the solid-liquid interface. This large availability of As(V) ions resulted in a rapid mass transfer and improved adsorption capacity [20].

Solution pH plays an important role in the adsorption of a pollutant over the adsorption surface. The variation in pH alters the adsorbent surface polarity and the distribution and speciation of As(V) in water. These alterations decide the adsorption capacity and interaction mechanism [24]. The effect of pH was studied in a broad pH range of 4–9 (Fig. 4**c**). The adsorption capacity significantly increased between pH 5–6, which was followed by a steep rise with the further increase in solution basicity. Similar pH-dependent profiles have been reported in previous studies as well [20]. Though the adsorption capacity was higher at high pH values, the adsorption capacity of 67 mg g^{-1} was maintained even at a low pH. The adsorption capacity of 86 mg g^{-1} at pH 7 suggested its

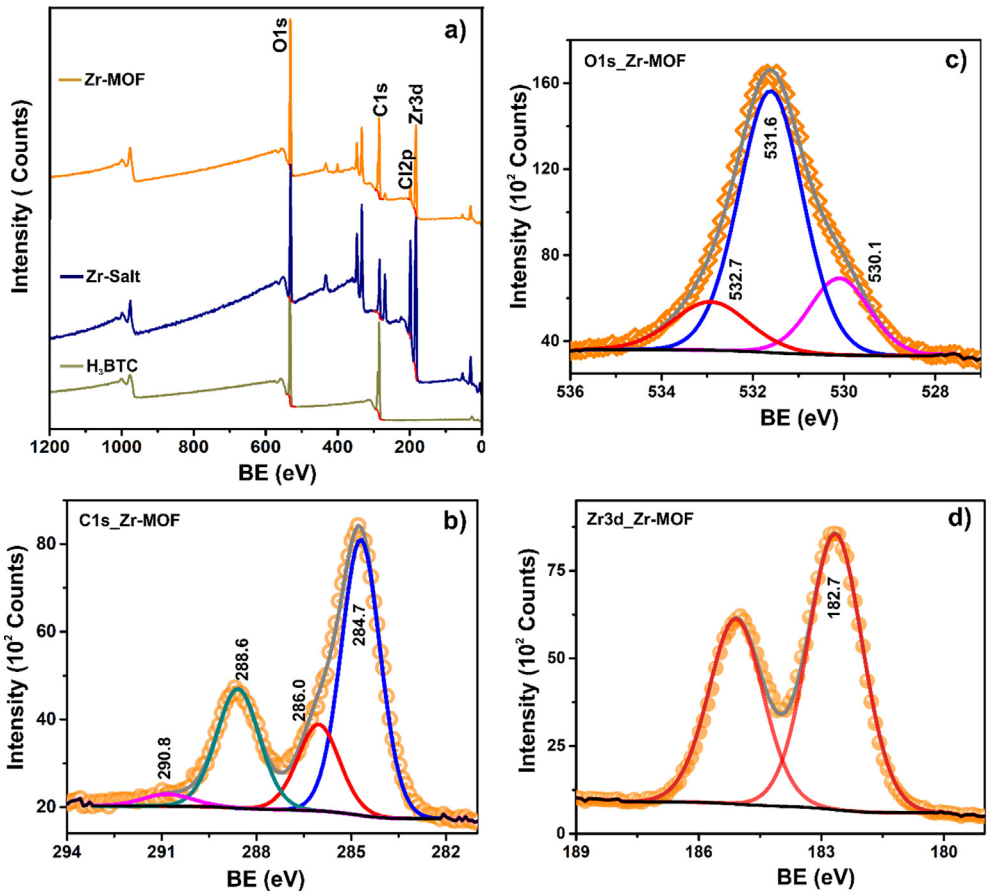

Fig. 2. (**a**) XPS survey spectra of Zr-MOF and precursors; high-resolution XPS (HRXPS) (**b**) C 1 s, (**c**) O 1 s, and (**d**) Zr 3d spectra of Zr-MOF.

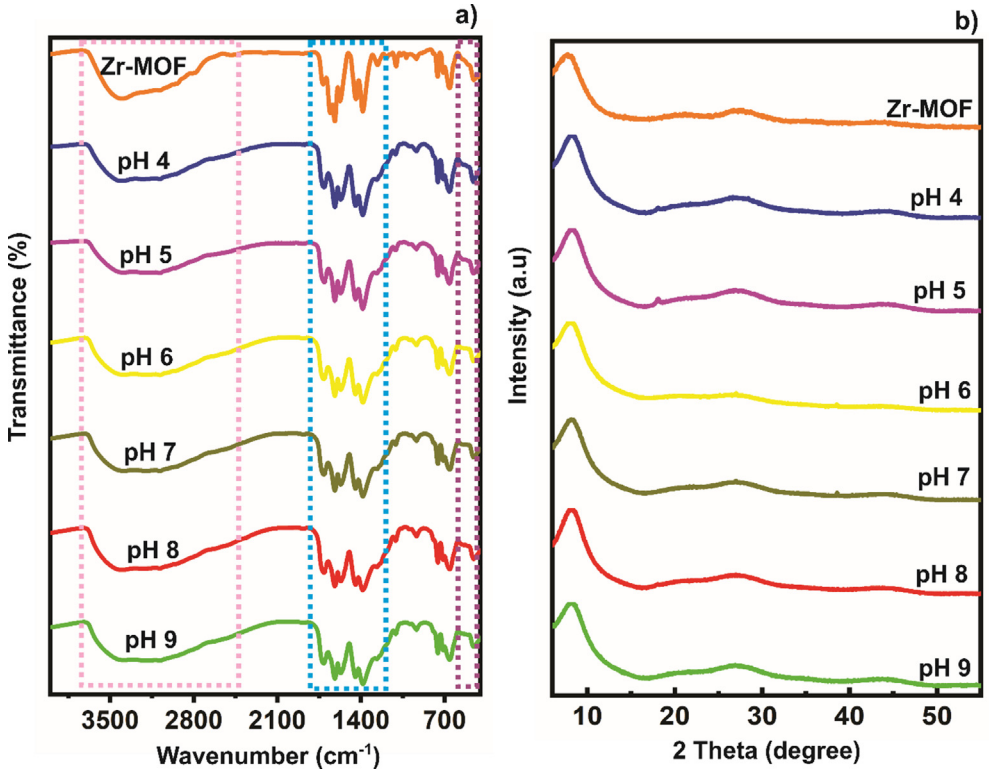

Fig. 3. (**a**) FTIR spectra and (**b**) PXRD patterns of Zr-MOF soaked in aqueous solutions at specific pH for 12 h.

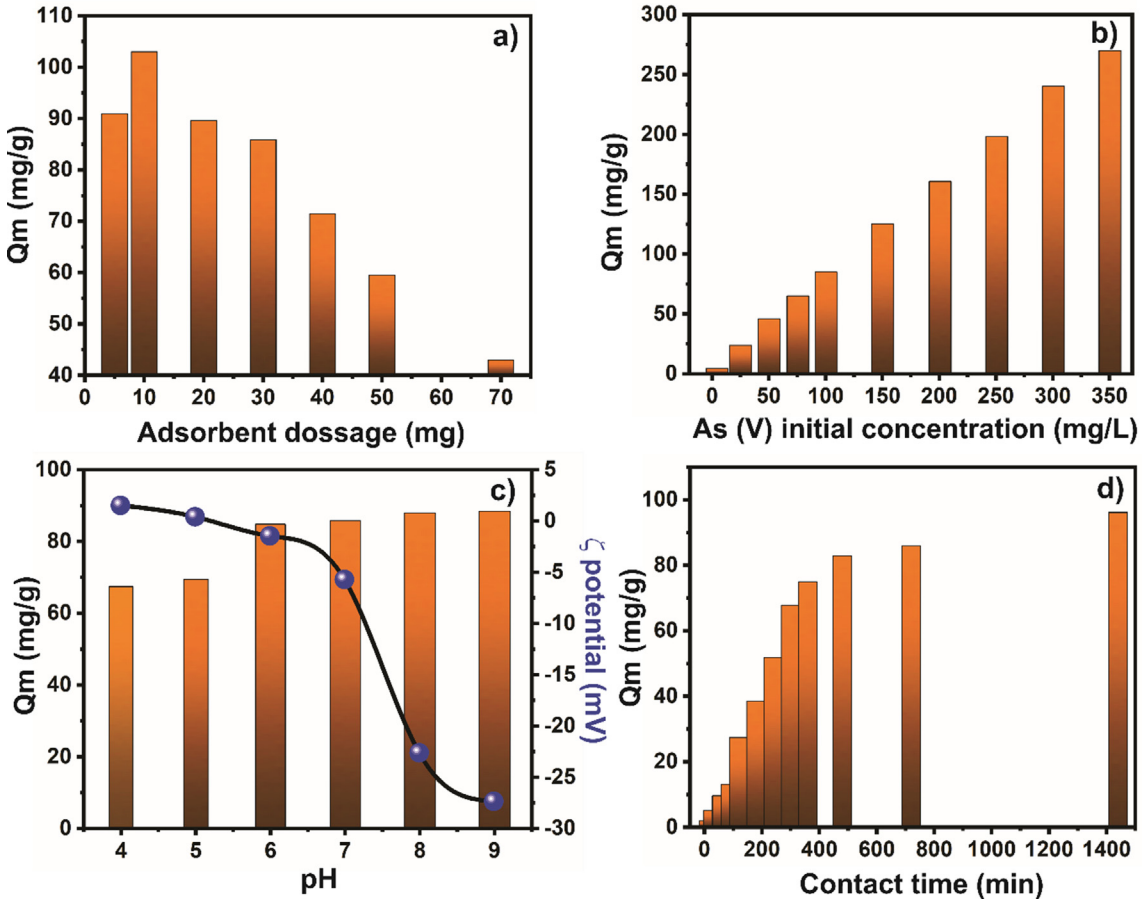

Fig. 4. Effect of (**a**) Adsorbent dosage; (**b**) As(V) concentration; (**c**) pH; (**d**) contact time on As(V) removal efficiency over Zr-MOF. Conditions: Zr-MOF mass = 30 mg, [As (V)] = 100 mg L^{-1}, volume = 30 mL, time = 12 h (changed accordingly).

applicability in the treatment of contaminated groundwater without pH alteration. The relationship between solution pH and the adsorption capacity of MOF could be established by identifying the MOF surface polarity and the speciation of As(V) ions as a function of pH. The zeta potential was measured as a function of pH, where the point of zero charges was ~5.6. Thus, the MOF surface was positively charged at pH < 5.6 and negatively charged at pH > 5.6. The speciation of arsenate is pH-dependent where H_3AsO_4 (at pH < 2.1), $H_2AsO_4^-$ (2.1 < pH < 6.7), and $HAsO_4^{2-}$ (pH > 6.7) predominates in the aqueous phase [20]. Though the MOF surface was slightly positive and the As(V) species was $H_2AsO_4^-$ in the pH range of 4–5, the adsorption capacity was comparatively low. At the same time, the adsorption capacity was high at a higher pH, even with a negatively charged surface and negatively charged As(V) species. Thus, it was evident that the electrostatic interaction was not responsible for the adsorption process. In neutral to alkaline solutions, the As(V) adsorption process is governed by the ligand-exchange mechanism [25]. As reported earlier, the adsorption of oxo-anions over Zr-based MOFs like UiO-66 [20,24] and MOF-808 [37] involves the substitution of terminal coordinated aqua or hydroxyl ligands on the Zr_6 clusters (Zr—OH/$Zr—OH_2$) with the oxyanions via monodentate and bidentate modes. The main adsorption pathway involves a ligand exchange of the bridging hydroxyl groups on the Zr-sites with the arsenate ions. Another pathway involved exchanging certain organic linkers of the MOF framework with arsenate leading to the formation of arsenic complexes. These binding modes have been investigated in the mechanism section in detail.

The arsenate uptake capacity as a function of contact time was studied for a long duration of 24 h (Fig. 4**d**). The adsorption capacity increased rapidly in the initial phase of the adsorption process (6 h), which was followed by a slow adsorption process in the remaining 18 h of contact time. By analyzing the time-dependent profile, it was evident that the large As(V) concentration gradient and abundant adsorption sites led to rapid adsorption in the initial phase. This was followed by the slowing of the adsorption process due to the low As(V) concentration near the solid-liquid interface and poor mass transfer phenomenon to access the internal adsorption sites.

The As(V) adsorption capacity of Zr-MOF was compared with the reported Zr-based based adsorbents in the literature (Table 1). The adsorption capacity of Zr-MOF (MOF-808) was more than 11 times higher than the one reported for MOF-808 [26]. The maximum As(V) adsorption capacity of 303.0 mg g^{-1} was reported for UiO-66 [24]. Though the adsorption capacity of our MOF is slightly low compared to that of UiO-66, the working pH of 2 and large stirring time of 48 h are the major drawbacks to the reported work. The MOF reported here is efficient in neutral pH solution and requires only 12 h of soaking.

3.4. Kinetics and isotherm

The PFO, PSO, Elovich, and IPD models were used to describe the adsorption kinetics (Fig. 5**a-d**). The equations of these models and parameters are listed in **Table S5**. The correlation coefficient (R^2) of PFO (0.95) was higher than the PSO (0.63) and Elovich model

Table 1
The adsorption capacity of reported Zr-based adsorbents for As(V) removal.

Adsorbent	Experimental conditions			q_e (mg g^{-1})
	pH	Dosage (g L^{-1})	Time (h)	
UiO-66 [24]	2.0	0.5	48	303.0
Zr-fumarate MOF [25]	6.8	1.0	12	230.3
Defected nanoscale UiO-66 [20]	7.0	1.0	3	200.0
Hierarchically porous UiO-66 [21]	6.0	0.05	7	248.8
UiO-66 [22]	9.2	1.0	24	68.2
UiO-66-NH_2 [41]	7.0	0.5	48	76.9
Fe_3O_4@UiO-66 [23]	7.0	0.2	4	33.1
MOF-808 [26]	–	0.2	4	24.8
Zr-immobilized nanoscale carbon [42]	2.5	1.0	48	110.0
Ceria-incorporated zirconia [43]	7.0	1.0	2	17.1
ZrO_2-immobilized alginate beads [44]	5.0	2.5	240	28.5
Zr-MOF [Present study]	7	1.0	12	278.0

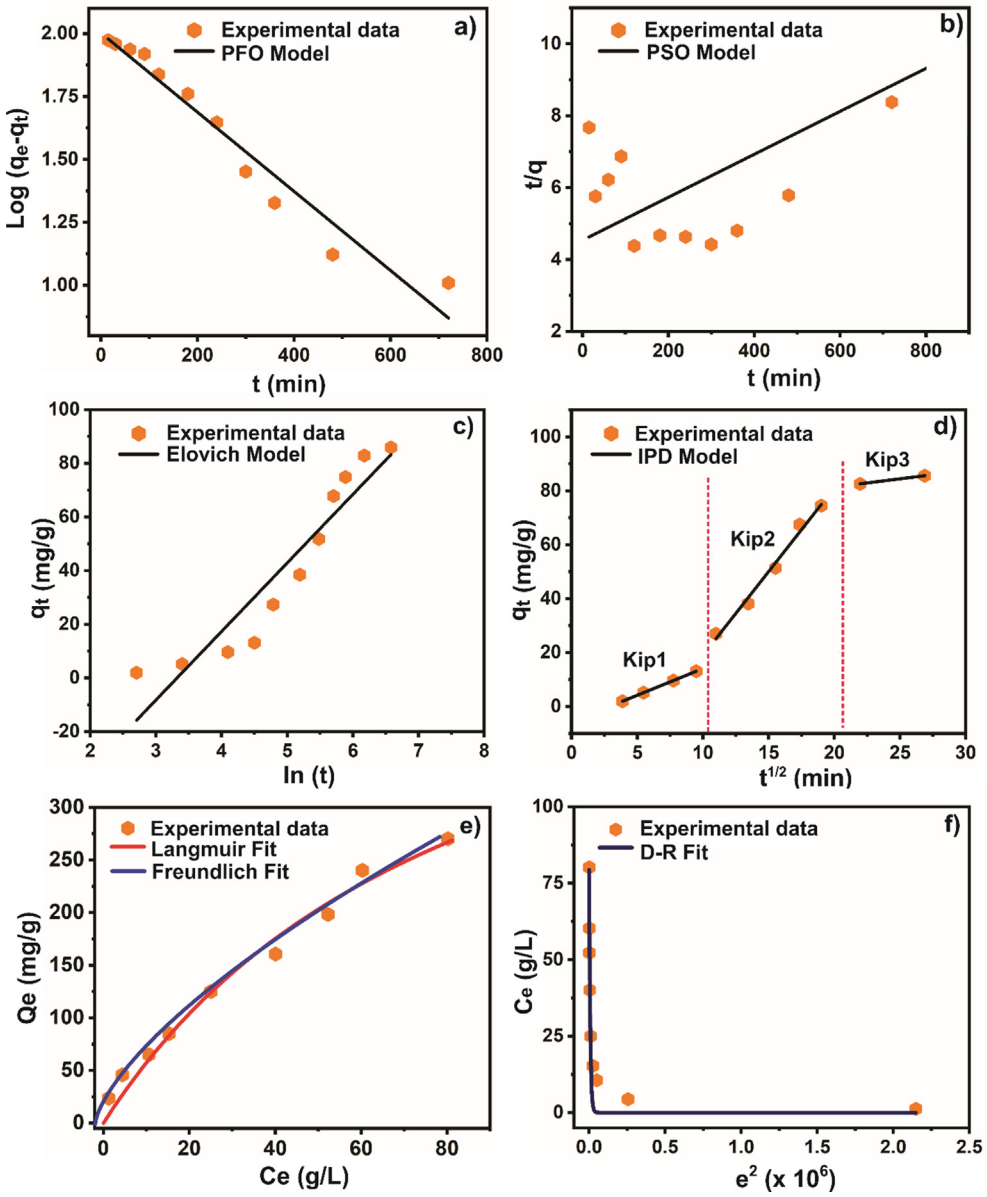

Fig. 5. (**a**) Pseudo-first-order (PFO); (**b**) pseudo-second-order (PSO); (**c**) Elovich; (**d**) intra-particle diffusion (IPD) kinetic fit; (**e**) Langmuir and Freundlich; (**f**) Dubinin-Radushkevich (D-R) isotherm fit for As (V) adsorption.

(0.91), which indicated that the As(V) adsorption kinetics followed the PFO model (**Table S6**). The intra-particle diffusion (IPD) model was employed to understand whether the diffusion mechanism played any role in the As(V) adsorption process. The kinetic data fitted in three regions, which were related to three adsorption processes for As(V) (Fig. 5**d**). The calculated rate constant (K_{ip}) followed the order: $K_{ip2} > K_{ip1} > K_{ip3}$ (**Table S6**). In the first step (K_{ip1}), the adsorption process started with the migration of As(V) ions from the bulk aqueous phase to the Zr-MOF surface. The second step (K_{ip2}) occurred after the saturation of the external surface. After saturation of external sites, As(V) ions entered the MOF pores with increasing resistance to diffusion. In the last step (K_{ip3}), arsenate diffused into the pores until the equilibrium was reached [20,38].

The experimental data were fitted with Langmuir, Freundlich, and D–R isotherm models to better understand the arsenic adsorption mechanism onto Zr-MOF (Fig. 5**e-f**, **Table S7**) [38]. The correlation coefficient value for the Freundlich model ($R^2 \sim 0.99$) and the Langmuir model ($R^2 \sim 0.98$) were close to unity. This suggested that the As(V) adsorption process was driven by physicochemical forces over MOF surface having sorption sites of different energies (**Table S8**) [45]. The separation factor (R_L) computed from the Langmuir model remained between 0 and 1, suggesting a favourable As (V) adsorption process over Zr-MOF. Moreover, the free Gibbs energy value was negative, which confirmed the spontaneity of the adsorption process [22].

3.5. Adsorption mechanism

The As(V) adsorption mechanism over Zr-MOF was probed using various spectroscopic techniques. The FTIR spectra of fresh and As(V)-loaded Zr-MOF are shown in Fig. 6**a**. The decreased broadness of the O—H band after As(V) adsorption hinted towards significant removal of hydrogen-bonded Zr—OH entities. This is the first indication of the involvement of these Zr-bound groups in the As(V) adsorption process. The relative decrease in the intensity of carboxylate bands suggested the replacement of some of the carboxylate linkers with the arsenate ions [24].

A more detailed investigation of the As(V) adsorption process over Zr-MOF was supported by XPS analysis. The HRXPS Zr 3d spectrum of Zr-MOF before and after As(V) adsorption is shown in Fig. 6**b**. The Zr $3d_{5/2}$ peak at 182.7 eV for fresh MOF shifted to 182.3 eV after As(V) adsorption. This shift to lower binding energy after As(V) adsorption has been reported in a previous study by He *et al* [22]. The shift in binding energy shift was due to the change in the electron density around the Zr-sites. The ligand-exchange mechanism involved the formation of the Zr—O—As bond via the substitution of Zr-coordinated hydroxyl groups by As(V) ions. Since the As—O group is more electronegative than O—H, the Zr-sites experienced a decrease in electron density after Zr—O—As formation, which was reflected as a shift in the Zr 3d binding energy [37]. The HRXPS O 1 s spectrum of Zr-MOF before and after As(V) adsorption is shown in Fig. 6**c**. The HRXPS O 1 s spectrum of As-adsorbed MOF has four contributions as opposed to three contributions observed for fresh MOF. The new peak at 531.3 eV was assigned to the Zr—O—As/As=O bonds. The peak at 533.3 eV was assigned to the As—OH bonds [46]. The peak at 532.7 eV for Zr—OH in the fresh MOF disappeared after the As(V) adsorption process. Thus, it was conclusive that the As(V) adsorption occurred on the protonated Zr—O(μ_3)—Zr sites, which provided Zr—OH for the substitution process. Another observation was the decreased Zr—O—C contribution in MOF from 63.5 to 45.0% after As(V) adsorption (**Table S3**). Wang *et al* predicted another possible As(V) interaction mode involving the Zr—O—C bond between Zr and linker. The adsorption could occur by forming Zr—O—As bonds at the expense of Zr—O—C(linker) bonds [24]. Although the reported work had no spectroscopic evidence to back the claim, the decreased Zr—O—C proportion after adsorption confirmed the breaking of the Zr—O—C bond and the formation of the Zr—O—As bond in this study. The HRXPS As 3d spectrum of As-adsorbed MOF was compared with the As 3d spectrum of NaH_2AsO_4 salt to ascertain the adsorbed As species over Zr-MOF, (Fig. 6**d**). In the HRXPS As 3d spectrum of As-adsorbed MOF, the contributions at 44.7 and 45.8 eV were assigned to the As $3d_{5/2}$ peak of As(III)—O and As(V)—O, respectively. Viltres *et al* have reported inconsistencies occurred during quantification of As oxidation states using the XPS analysis. The exposure to X-ray during XPS analysis could lead to the formation of As(III) species, which is wrongly interpreted as a reduction of As (V) species during the experimental phase [46]. The same observation was recorded in the HRXPS As 3d spectrum of NaH_2AsO_4 salt, which showed a presence of 4.6% of As in the trivalent state (**Table S9**). But, the large proportion of As(III) ions (23.3%) in Zr-MOF could not be from the X-ray exposure alone and was conclusive of the partial reduction of As(V) species to As(III) during the adsorption process.

3.6. DFT calculations

Since the bulk phase of MOF-808 contains identical structural units (Fig. 7**a**), we have considered the single building unit of MOF-808 and performed the structural optimization to reduce the computational cost and time. The computed optimized structure of a single building unit of MOF-808 is depicted in Fig. 7**b**. In Fig. 7**b**, the bond length C—C (close to O), C—C (in C ring), C—H, C—O (close to H), C—O (close to O), C—O (close to Zr), Zr—O (close to C), Zr—O (close to Zr), Zr—O (close to H), and O—H is 1.49, 1.40, 1.09, 1.25, 1.29, 1.27, 2.24, 2.09, 2.27, and 0.96 Å, respectively.

We have studied As(V) adsorption via different modes on the relaxed structure of a single building unit of MOF-808. To understand the adsorption mechanism involving the breaking of framework bonds, followed by the adsorption of As(V) ions, we have considered two specific sites on a single building unit of MOF-808. Which were represented as A (breaking of Zr—O(carboxylate)) and B (ligand exchange with the Zr—(μ_3-OH) bridges), indicated in Fig. 7**b**. These two binding modes were proposed by Wang *et al* [24]. We have computed the optimized geometry, binding energy, and Zr—O(As) bond length shown in Fig. 8. On-site A, a single unit of MOF-808 remained identical, and As(V) ions bound to the two Zr-sites as a mononuclear bidentate complex after the breaking of two Zr—O(carboxylate) bonds. The computed Zr—O(As) bond length was 2.14 Å, and the binding energy was 4.11 eV. Slight distortion in the single unit of MOF-808 was noticed due to the breaking of framework Zr—O(carboxylate bonds). The B configuration involved the ligand-exchange mechanism of —OH groups on the Zr—(μ_3-OH) bridges with As(V) ions. The computed bond length and binding energy were calculated as 2.42 Å and 4.38 eV, respectively. Among sites A and B, the maximum binding energy was obtained for site B. For this reason, it was the most preferred site for As(V) adsorption onto the MOF, which is also strongly backed by the spectroscopic analysis.

Furthermore, we have also studied the direct interaction of As (V) ions on a single unit of MOF-808, labelled as a C site in Fig. 7**b**. The optimized structure for As(V) adsorption is depicted in Fig. 8. For this configuration, we have calculated the binding energy and bond length as 0.84 eV and 2.36 Å, respectively. The computed binding energy for the C site is much lesser than that of the A and B sites. Thus, based on energy considerations, the direct interaction of As(V) with the Zr-sites (C site) was unfavourable, and the ligand-exchange (B site) mechanism was the most favourable mechanism involved in the As(V) adsorption process.

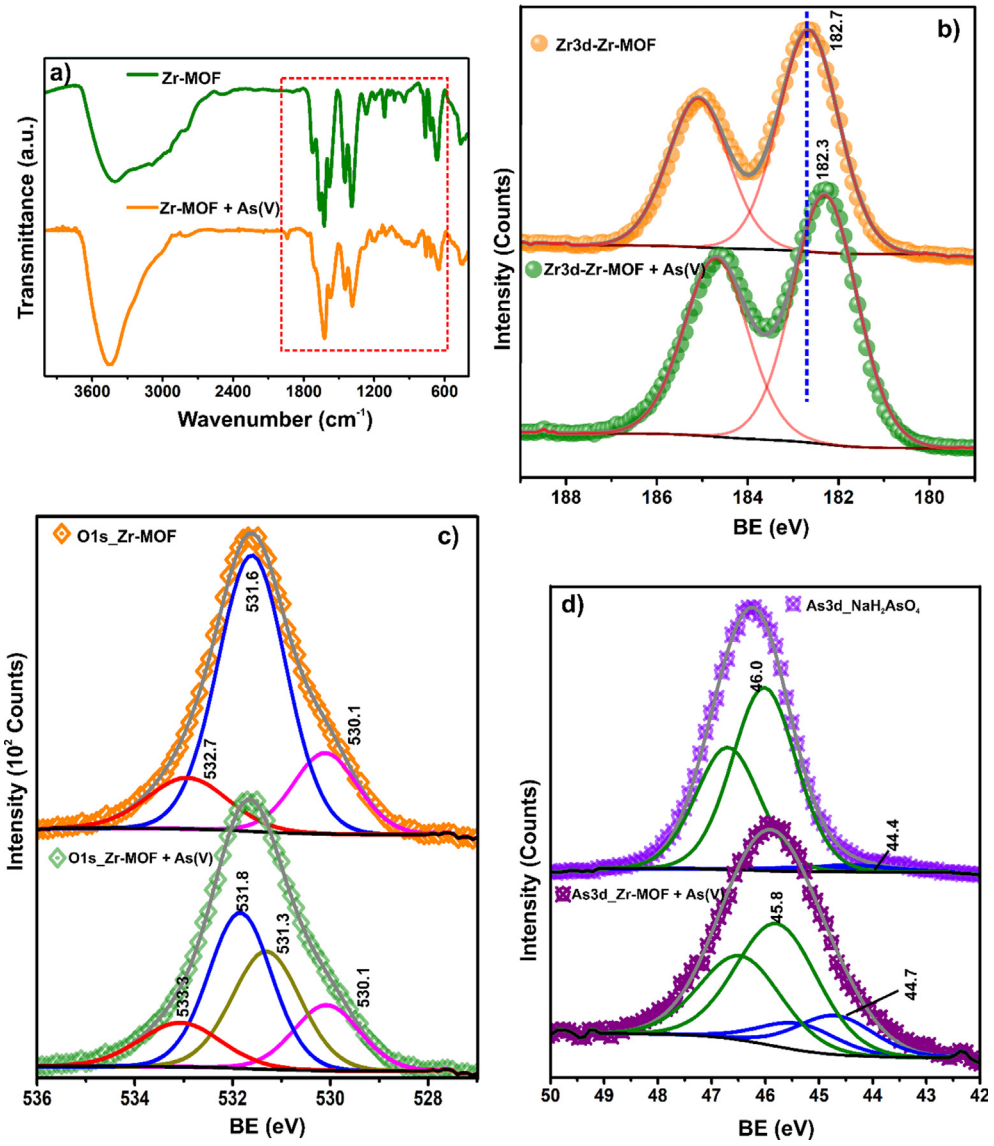

Fig. 6. (**a**) FTIR spectra; (**b**) Raman spectra; HRXPS (**c**) Zr 3d; (**d**) O 1 s spectra of Zr-MOF before and after As(V) adsorption; (**e**) As 3d spectra of NaH_2AsO_4 and As(V)-loaded Zr-MOF.

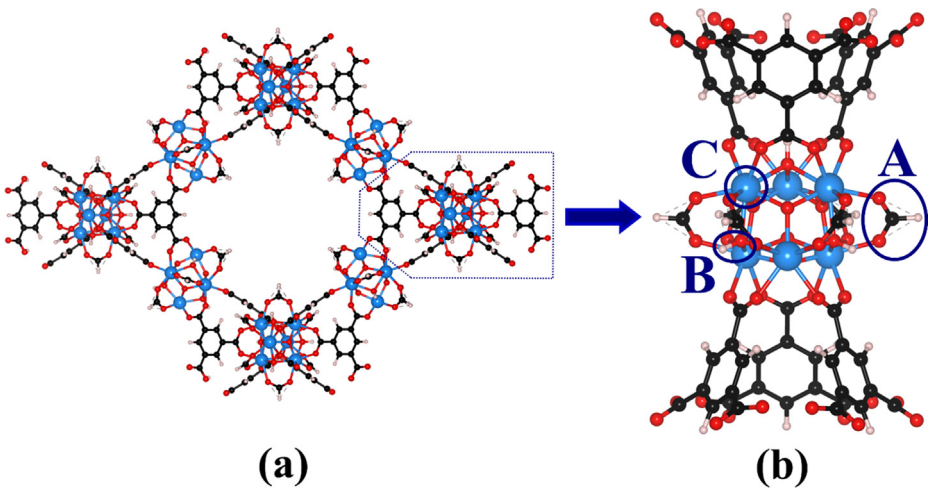

Fig. 7. **(a)** Structure of MOF-808, **(b)** optimized single building unit of MOF-808. Here A, B, and C indicate the possible binding sites on a single building unit of MOF-808. Colour codes: Carbon (black), Zirconium (blue), Oxygen (red), and Hydrogen (white). (For interpretation of the references to colour in this figure legend, the reader is referred to the web version of this article.)

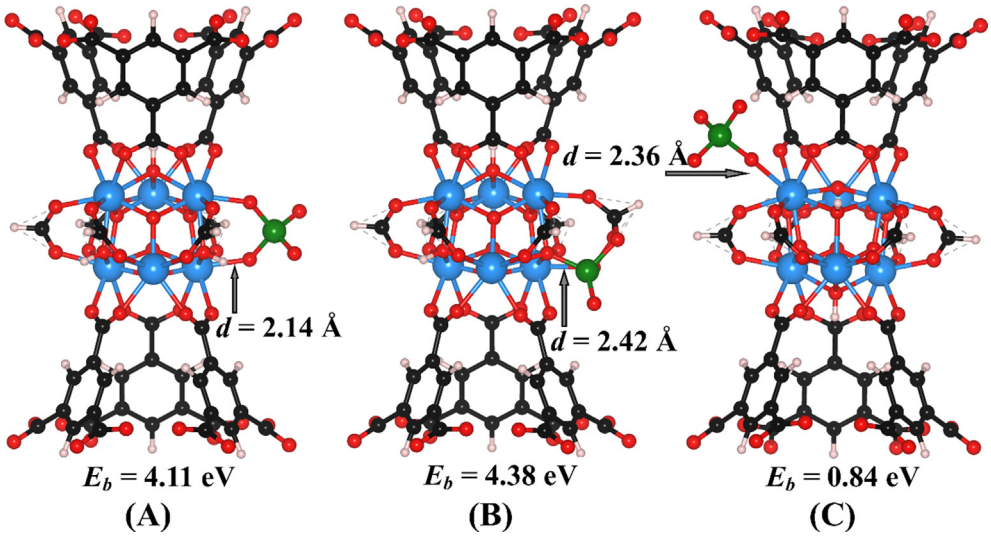

Fig. 8. Adsorption of As(V) ions on single building unit of MOF-808. For the respective configurations, their binding energy and the Zr—O(As) bond length are reported. Colour codes: Carbon (black), Zirconium (blue), Oxygen (red), Hydrogen (white), and Arsenic (green). (For interpretation of the references to colour in this figure legend, the reader is referred to the web version of this article.)

3.7. Co-adsorption of cations

Like anionic removal applications, Zr-based MOFs have been explored for the removal of cationic heavy metals like Cd(II) [47] and Pb(II) [48]. Since industrial wastewater and even contaminated groundwater have a matrix of heavy metals and alkaline earth metals, it is required that the single MOF should be able to remove these cationic and anionic metal species simultaneously. Moreover, the presence of additional pollutants may reduce the As(V) removal capacity of the MOF. The literature has established that other than phosphates, no other anion interferes with the As (V) adsorption process [22]. Darezereshki *et al* reported a decrease in the As(V) removal performance of magnetite in the presence of divalent and trivalent heavy metal cations [49]. In the present case, we have studied the simultaneous removal of As(V), heavy metals, and alkaline earth metal ions (Fig. 9**a**). In the complex solution of ions, Zr-MOF could effectively adsorb As(V), Cd(II), Fe(III), Pb(II), Ca(II), and Mg(II), where the adsorption capacity was 93.8, 38.8, 36.5, 43.6, 57.7, and 44.7 mg g^{-1}, respectively. As(V) adsorption breakthrough curve in a multi-element solution (As, Cd, Fe, Pb, Ca, and Mg) is shown in Fig. 9**b**. The breakthrough curve demonstrated that 25 mL of the contaminated water was filtered by the adsorbent bed without any trace of As(V) ion in the effluent solution. Thus the breakthrough capacity was calculated to be 3.43 mg g^{-1}. After this, the presence of As(V) in the effluent water was observed and the material was fully consumed after passing 60 mL of the contaminated water with the maximum exhaustive capacity of 5.61 mg g^{-1}.

3.8. Reusability

Regeneration and reusability are important criteria to judge the adsorption process on the grounds of affordability and sustainability. The eluent for stripping As(V) from the loaded MOF should be economical, non-toxic, and non-corrosive to the MOF. In general, the use of an acid or a base (pH swing method) is highly sought after eluent for the stripping of arsenate [25,50]. In the present work, we have studied both HCl and NaOH as eluents for regeneration purposes. The adsorption and desorption efficiency of Zr-MOF with HCl and NaOH are shown in Fig. 10. Since low adsorption

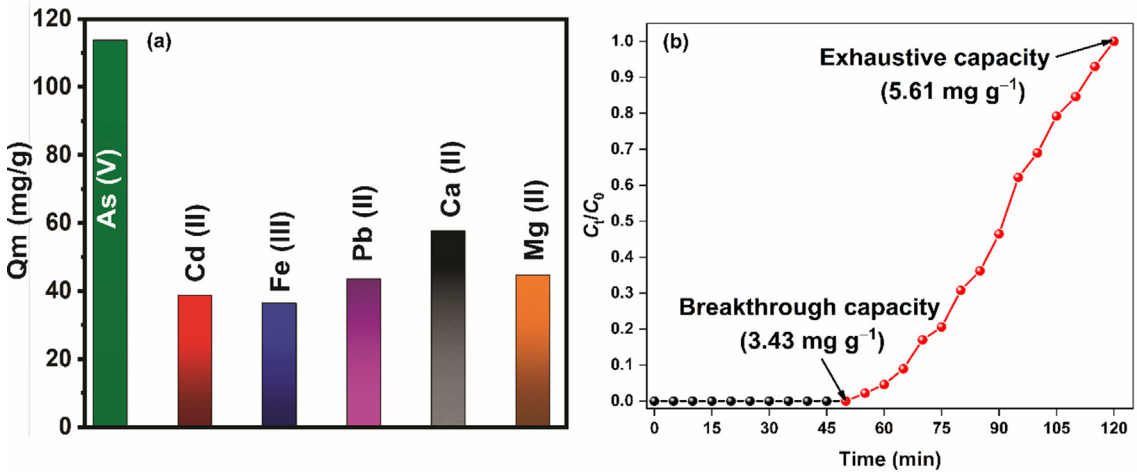

Fig. 9. (**a**) Removal performance of As(V) and other cations. Conditions: Mass = 30 mg, [Ion] = 100 mg L^{-1} each, volume = 30 mL, time = 12 h. (**b**) Breakthrough curve for As(V) adsorption in a multi-element study. Conditions: Mass = 40 mg, [Ion] = 5 mg L^{-1} each, flowrate = 0.5 mL min^{-1}.

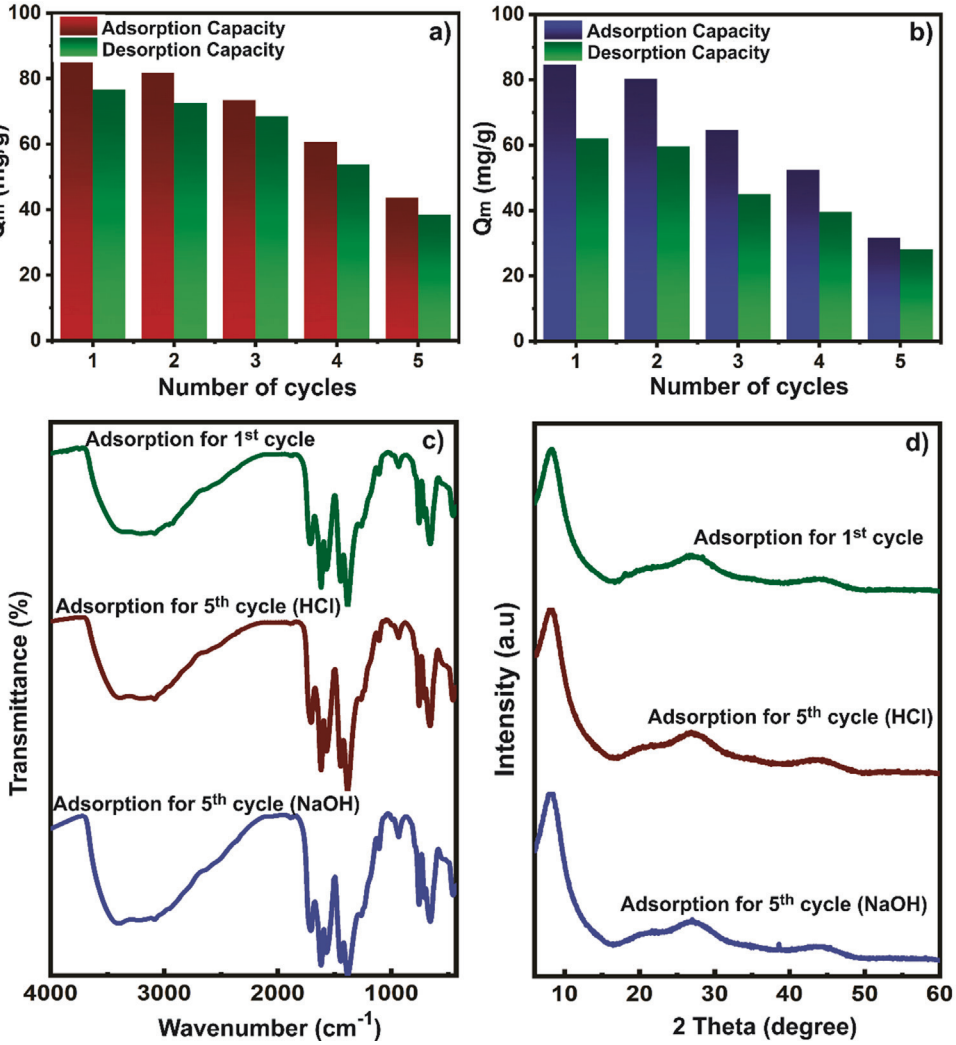

Fig. 10. Regeneration and reusability tests of Zr-MOF with (**a**) HCl; (**b**) NaOH; (c) FTIR spectra and (**d**) PXRD patterns of Zr-MOF after reusability test. Conditions: Mass = 30 mg, [As(V)] = 100 mg L^{-1}, [NaOH]/[HCl] = 0.1 mol L^{-1}, volume = 30 mL, time = 12 h.

capacity was observed in the acidic range, HCl as the stripping agent was effective in stripping out the sorbed As(V) ions. A ~90% desorption efficiency in each cycle failed to regenerate all the adsorption sites in the Zr-MOF, which was reflected as decreased adsorption capacity in subsequent cycles. Though the adsorption capacity gradually decreased with the increasing number of cycles, the adsorption capacity was still favourable till the 5th cycle (Fig. 10**a**). NaOH as eluent showed poor regenerability compared to HCl (Fig. 10**b**). Since the desorption efficiency was less convincing, the adsorption-desorption capacity in subsequent cycles was even lower than observed for HCl. Thus, it was confirmed that HCl was the suitable eluent, and Zr-MOF was highly efficient in As(V) removal for multiple cycles.

The stability of Zr-MOF after multiple adsorption-desorption cycles was probed using FTIR and PXRD analysis. In the 5th adsorption cycle, the FTIR spectra of Zr-MOF overlapped with the FTIR spectrum of the 1st adsorption cycle. Moreover, no significant difference was observed in the spectra with NaOH or HCl as eluent (Fig. 10**c**). In the PXRD pattern of Zr-MOF (5th adsorption cycle NaOH), the two low-intensity peaks observed at 27.5° and 38.5° were assigned to the −111 and 120 reflections of monoclinic ZrO_2 (ICDD File No. 37-1484) [51]. The ZrO_2 formed due to the precipitating effect of NaOH. The diffraction peaks corresponding to ZrO_2 were absent in Zr-MOF when HCl was used as the eluent (Fig. 10**d**). Thus, the stability of Zr-sites in MOF during regeneration with HCl was partly responsible for its better efficacy than NaOH.

4. Conclusion

In the present work, we have reported zirconium trimesate MOF (Zr-MOF) for the adsorptive removal of As(V) ions from an aqueous solution. The synthesized MOF was characterized by various spectroscopic techniques to evaluate its physicochemical properties. The MOF showed appreciable adsorption capacity in the pH range of 4–9 with higher adsorption capacity in the basic condition due to the ligand-exchange process. The maximum adsorption capacity of 278 mg g^{-1} was comparable to the reported values of UiO-66 MOF in the literature. The adsorption process was driven by a diffusion mechanism on a heterogeneous surface involving physicochemical forces. FTIR and XPS analysis confirmed two adsorption pathways for As(V) adsorption involving Zr—OH (μ_3)—Zr and Zr—O—C (linker) sites. These adsorption pathways were strongly backed by DFT calculations. The XPS analysis also confirmed the presence of As(III) formed due to the reduction of As(V) species. The MOF showed significantly high adsorption capacity for cations and As(V) ions in a multi-element solution. The Zr-MOF was successfully regenerated by 0.1 mol L^{-1} HCl solu-

tion without compromising with the MOF structural integrity. Thus, the study presents Zr-MOF as a novel adsorbent for the treatment of As-contaminated wastewater.

CRediT authorship contribution statement

Roxana Paz: Formal analysis. **Herlys Viltres:** Investigation, Conceptualization, Data curation. **Nishesh Kumar Gupta:** Visualization, Data curation, Formal analysis. **Kaptan Rajput:** Visualization, Data curation, Formal analysis. **Debesh R. Roy:** Data curation, Formal analysis. **Adolfo Romero-Galarza:** Data curation, Formal analysis. **Mark C. Biesinger:** Data curation, Formal analysis. **Carolina Leyva:** Investigation, Visualization, Conceptualization, Project administration.

Declaration of Competing Interest

The authors declare that they have no known competing financial interests or personal relationships that could have appeared to influence the work reported in this paper.

Acknowledgement

The authors would like to thank Laboratorio Nacional de Ciencia, Tecnología y Gestión Integrada del Agua (LNAGUA) and LNCAE (Laboratorio Nacional de Conversión y Almacenamiento de Energía) for their experimental and instrument facilities.

Appendix A. Supplementary material

Supplementary data to this article can be found online at https://doi.org/10.1016/j.molliq.2022.118957.

References

[1] D. Mohanty, Conventional as well as emerging arsenic removal technologies—A critical review, Water Air Soil Pollut. 228 (2017) 381, https://doi.org/10.1007/s11270-017-3549-4.
[2] W. Yu, M. Luo, Y. Yang, H. Wu, W. Huang, K. Zeng, F. Luo, Metal-organic framework (MOF) showing both ultrahigh As(V) and As(III) removal from aqueous solution, J. Solid State Chem. 269 (2019) 264–270, https://doi.org/10.1016/j.jssc.2018.09.042.
[3] T. Shahryari, F. Vahidipour, N.P.S. Chauhan, G. Sargazi, Synthesis of a novel Zn-MOF/PVA nanofibrous composite as bioorganic material: Design, systematic study and an efficient arsenic removal, Polym. Eng. Sci. 60 (2020) 2793–2803, https://doi.org/10.1002/pen.25510.
[4] WHO, World Health Organization, Preventing Disease through Healthy Environment. Exposure to Arsenic: A Major Public Health Concern, Prev. Dis. through Heal. Environ. (2019) 1–5. http://www.who.int/ipcs/features/arsenic.pdf?ua=1.
[5] H. Wu, M.D. Ma, W.Z. Gai, H. Yang, J.G. Zhou, Z. Cheng, P. Xu, Z.Y. Deng, Arsenic removal from water by metal-organic framework MIL-88A microrods, Environ. Sci. Pollut. Res. 25 (2018) 27196–27202, https://doi.org/10.1007/s11356-018-2751-2.
[6] J. Sun, X. Zhang, A. Zhang, C. Liao, Preparation of Fe–Co based MOF-74 and its effective adsorption of arsenic from aqueous solution, J. Environ. Sci. (China) 80 (2019) 197–207, https://doi.org/10.1016/j.jes.2018.12.013.
[7] Y. Wang, C. Lv, L. Xiao, G. Fu, Y. Liu, S. Ye, Y. Chen, Arsenic removal from alkaline leaching solution using Fe (III) precipitation, Environ. Technol. (United Kingdom) 40 (2019) 1714–1720, https://doi.org/10.1080/09593330.2018.1429495.
[8] C. Corroto, A. Iriel, A.F. Cirelli, A.L.P. Carrera, Constructed wetlands as an alternative for arsenic removal from reverse osmosis effluent, Sci. Total Environ. 691 (2019) 1242–1250, https://doi.org/10.1016/j.scitotenv.2019.07.234.
[9] A. Chiavola, E. D'Amato, R. Gavasci, P. Sirini, Arsenic removal from groundwater by ion exchange and adsorption processes: Comparison of two different materials, Water Sci. Technol. Water Supply. 15 (2015) 981–989, https://doi.org/10.2166/ws.2015.054.
[10] M. López-Guzmán, M.T. Alarcón-Herrera, J.R. Irigoyen-Campuzano, L.A. Torres-Castañón, L. Reynoso-Cuevas, Simultaneous removal of fluoride and arsenic from well water by electrocoagulation, Sci. Total Environ. 678 (2019) 181–187, https://doi.org/10.1016/j.scitotenv.2019.04.400.
[11] M. Imran, M.M. Iqbal, J. Iqbal, N.S. Shah, Z.U.H. Khan, B. Murtaza, M. Amjad, S. Ali, M. Rizwan, Synthesis, characterization and application of novel MnO and CuO impregnated biochar composites to sequester arsenic (As) from water: Modeling, thermodynamics and reusability, J. Hazard. Mater. 401 (2021), https://doi.org/10.1016/j.jhazmat.2020.123338 123338.
[12] S.I. Siddiqui, M. Naushad, S.A. Chaudhry, Promising prospects of nanomaterials for arsenic water remediation: A comprehensive review, Process Saf. Environ. Prot. 126 (2019) 60–97, https://doi.org/10.1016/j.psep.2019.03.037.
[13] M.M. Hussain, J. Wang, I. Bibi, M. Shahid, N.K. Niazi, J. Iqbal, I.A. Mian, S.M. Shaheen, S. Bashir, N.S. Shah, K. Hina, J. Rinklebe, Arsenic speciation and biotransformation pathways in the aquatic ecosystem: The significance of algae, J. Hazard. Mater. 403 (2021), https://doi.org/10.1016/j.jhazmat.2020.124027 124027.
[14] S. Alka, S. Shahir, N. Ibrahim, M.J. Ndejiko, D.V.N. Vo, F.A. Manan, Arsenic removal technologies and future trends: A mini review, J. Clean. Prod. 278 (2021), https://doi.org/10.1016/j.jclepro.2020.123805 123805.
[15] H. Viltres, Y.C. López, N.K. Gupta, C. Leyva, R. Paz, A. Gupta, A. Sengupta, Functional metal-organic frameworks for metal removal from aqueous solutions, Sep. Purif. Rev. 51 (2022) 78–99, https://doi.org/10.1080/15422119.2020.1839909.
[16] Y.C. López, H. Viltres, N.K. Gupta, P. Acevedo-Peña, C. Leyva, Y. Ghaffari, A. Gupta, S. Kim, J. Bae, K.S. Kim, Transition metal-based metal-organic frameworks for environmental applications: a review, Environ. Chem. Lett. 19 (2021) 1295–1334, https://doi.org/10.1007/s10311-020-01119-1.
[17] S. Sonal, B.K. Mishra, A comprehensive review on the synthesis and performance of different zirconium-based adsorbents for the removal of various water contaminants, Chem. Eng. J. 424 (2021), https://doi.org/10.1016/j.cej.2021.130509 130509.
[18] M.A. Rahman, D. Lamb, M.M. Rahman, M.M. Bahar, P. Sanderson, S. Abbasi, A.S. M.F. Bari, R. Naidu, Removal of arsenate from contaminated waters by novel zirconium and zirconium-iron modified biochar, J. Hazard. Mater. 409 (2021), https://doi.org/10.1016/j.jhazmat.2020.124488 124488.
[19] J. Hou, H. Wang, H. Zhang, Zirconium metal-organic framework materials for efficient ion adsorption and sieving, Ind. Eng. Chem. Res. 59 (2020) 12907–12923, https://doi.org/10.1021/acs.iecr.0c02683.
[20] N. Assaad, G. Sabeh, M. Hmadeh, Defect control in Zr-based metal-organic framework nanoparticles for arsenic removal from water, ACS Appl. Nano Mater. 3 (2020) 8997–9008, https://doi.org/10.1021/acsanm.0c01696.
[21] R. Xu, Q. Ji, P. Zhao, M. Jian, C. Xiang, C. Hu, G. Zhang, C. Tang, R. Liu, X. Zhang, J. Qu, Hierarchically porous UiO-66 with tunable mesopores and oxygen vacancies for enhanced arsenic removal, J. Mater. Chem. A 8 (2020) 7870–7879, https://doi.org/10.1039/c9ta13747e.
[22] X. He, F. Deng, T. Shen, L. Yang, D. Chen, J. Luo, X. Luo, X. Min, F. Wang, Exceptional adsorption of arsenic by zirconium metal-organic frameworks: Engineering exploration and mechanism insight, J. Colloid Interface Sci. 539 (2019) 223–234, https://doi.org/10.1016/j.jcis.2018.12.065.
[23] J.B. Huo, L. Xu, X. Chen, Y. Zhang, J.C.E. Yang, B. Yuan, M.L. Fu, Direct epitaxial synthesis of magnetic Fe_3O_4@UiO-66 composite for efficient removal of arsenate from water, Microporous Mesoporous Mater. 276 (2019) 68–75, https://doi.org/10.1016/j.micromeso.2018.09.017.
[24] C. Wang, X. Liu, J.P. Chen, K. Li, Superior removal of arsenic from water with zirconium metal-organic framework UiO-66, Sci. Rep. 5 (2015) 1–10, https://doi.org/10.1038/srep16613.
[25] S. Muthu Prabhu, S. Kancharla, C.M. Park, K. Sasaki, Synthesis of modulator-driven highly stable zirconium-fumarate frameworks and mechanistic investigations of their arsenite and arsenate adsorption from aqueous solutions, CrystEngComm 21 (2019) 2320–2332, https://doi.org/10.1039/C8CE01424H.
[26] Z.Q. Li, J.C. Yang, K.W. Sui, N. Yin, Facile synthesis of metal-organic framework MOF-808 for arsenic removal, Mater. Lett. 160 (2015) 412–414, https://doi.org/10.1016/j.matlet.2015.08.004.
[27] H. Furukawa, F. Gándara, Y.B. Zhang, J. Jiang, W.L. Queen, M.R. Hudson, O.M. Yaghi, Water adsorption in porous metal-organic frameworks and related materials, J. Am. Chem. Soc. 136 (2014) 4369–4381, https://doi.org/10.1021/ja500330a.
[28] C. Ardila-Suárez, J. Rodríguez-Pereira, V.G. Baldovino-Medrano, G.E. Ramírez-Caballero, An analysis of the effect of zirconium precursors of MOF-808 on its thermal stability, and structural and surface properties, CrystEngComm 21 (2019) 1407–1415, https://doi.org/10.1039/c8ce01722k.
[29] R.S. Andriamitantsoa, W. Dong, H. Gao, G. Wang, Porous organic-inorganic hybrid xerogels for stearic acid shape-stabilized phase change materials, New J. Chem. 41 (2017) 1790–1797, https://doi.org/10.1039/c6nj03034c.
[30] B.H. Park, Y. Jung, S. Kim, Particle size control influence on the electrochemical properties of sulfur deposited on metal organic frameworks host electrodes, J. Inorg. Organomet. Polym Mater. 31 (2021) 1931–1938, https://doi.org/10.1007/s10904-021-01901-w.
[31] C. Ardila-Suárez, A.M. Díaz-Lasprilla, L.A. Díaz-Vaca, P.B. Balbuena, V.G. Baldovino-Medrano, G.E. Ramírez-Caballero, Synthesis, characterization, and post-synthetic modification of a micro/mesoporous zirconium-tricarboxylate metal-organic framework: Towards the addition of acid active sites, CrystEngComm 21 (2019) 3014–3030, https://doi.org/10.1039/c9ce00218a.
[32] M. Todaro, A. Alessi, L. Sciortino, S. Agnello, M. Cannas, F.M. Gelardi, G. Buscarino, Investigation by raman spectroscopy of the decomposition process of HKUST-1 upon exposure to air, J. Spectrosc. 2016 (2016) 8074297, https://doi.org/10.1155/2016/8074297.
[33] K. Doloi, A. Kumar, M.N. Rao, Study of polymerization dynamics in micropores of metal-organic framework, AIP Conf. Proc. 2265 (2020), https://doi.org/10.1063/5.0017416 030013.

[34] K. Knozowska, R. Thür, J. Kujawa, I. Kolesnyk, I.F.J. Vankelecom, W. Kujawski, Fluorinated MOF-808 with various modulators to fabricate high-performance hybrid membranes with enhanced hydrophobicity for organic-organic pervaporation, Sep. Purif. Technol. 264 (2021), https://doi.org/10.1016/j.seppur.2021.118315 118315.
[35] E. Plessers, G. Fu, C.Y.X. Tan, D.E. De Vos, M.B.J. Roeffaers, Zr-based MOF-808 as meerwein–ponndorf–verley reduction catalyst for challenging carbonyl compounds, Catalysts. 6 (2016) 104, https://doi.org/10.3390/catal6070104.
[36] N. Torres, J. Galicia, Y. Plasencia, A. Cano, F. Echevarría, L.F. Desdin-Garcia, E. Reguera, Implications of structural differences between Cu-BTC and Fe-BTC on their hydrogen storage capacity, Colloids Surfaces A Physicochem. Eng. Asp. 549 (2018) 138–146, https://doi.org/10.1016/j.colsurfa.2018.04.016.
[37] Z.J. Lin, H.Q. Zheng, Y.N. Zeng, Y.L. Wang, J. Chen, G.J. Cao, J.F. Gu, B. Chen, Effective and selective adsorption of organoarsenic acids from water over a Zr-based metal-organic framework, Chem. Eng. J. 378 (2019), https://doi.org/10.1016/j.cej.2019.122196 122196.
[38] R. Paz, H. Viltres, Y.C. López, N. Kumar Gupta, C. Levya, Fabrication of magnetic cerium-organic framework-activated carbon composite for charged dye removal from aqueous solutions, J. Mol. Liq. 337 (2021), https://doi.org/10.1016/j.molliq.2021.116578 116578.
[39] T. Sreethawong, S. Ngamsinlapasathian, S. Yoshikawa, Synthesis of crystalline mesoporous-assembled ZrO_2 nanoparticles via a facile surfactant-aided sol-gel process and their photocatalytic dye degradation activity, Chem. Eng. J. 228 (2013) 256–262, https://doi.org/10.1016/j.cej.2013.04.111.
[40] A.S. Sartape, A.M. Mandhare, V.V. Jadhav, P.D. Raut, M.A. Anuse, S.S. Kolekar, Removal of malachite green dye from aqueous solution with adsorption technique using Limonia acidissima (wood apple) shell as low cost adsorbent, Arab. J. Chem. 10 (2017) S3229–S3238, https://doi.org/10.1016/j.arabjc.2013.12.019.
[41] Z.W. Chang, Y.J. Lee, D.J. Lee, Adsorption of hydrogen arsenate and dihydrogen arsenate ions from neutral water by UiO-66-NH_2, J. Environ. Manage. 247 (2019) 263–268, https://doi.org/10.1016/j.jenvman.2019.06.068.
[42] N. Mahanta, J.P. Chen, A novel route to the engineering of zirconium immobilized nano-scale carbon for arsenate removal from water, J. Mater. Chem. A 1 (2013) 8636–8644, https://doi.org/10.1039/c3ta10858a.
[43] A. Ghosh, S. Kanrar, D. Nandi, P. Sasikumar, K. Biswas, U.C. Ghosh, Redox-assisted arsenic(III) adsorption for removal from aqueous solution by cerium (IV)-incorporated zirconium oxide nanocomposites, J. Chem. Eng. Data 65 (2020) 885–895, https://doi.org/10.1021/acs.jced.9b01075.
[44] O.H. Kwon, J.O. Kim, D.W. Cho, R. Kumar, S.H. Baek, M.B. Kurade, B.H. Jeon, Adsorption of As(III), As(V) and Cu(II) on zirconium oxide immobilized alginate beads in aqueous phase, Chemosphere 160 (2016) 126–133, https://doi.org/10.1016/j.chemosphere.2016.06.074.
[45] Y.K. Penke, G. Anantharaman, J. Ramkumar, K.K. Kar, Aluminum substituted cobalt ferrite (Co−Al−Fe) nano adsorbent for arsenic adsorption in aqueous systems and detailed redox behavior study with XPS, ACS Appl. Mater. Interfaces 9 (2017) 11587–11598, https://doi.org/10.1021/acsami.6b16414.
[46] H. Viltres, O.F. Odio, L. Lartundo-Rojas, E. Reguera, Degradation study of arsenic oxides under XPS measurements, Appl. Surf. Sci. 511 (2020), https://doi.org/10.1016/j.apsusc.2020.145606 145606.
[47] J. Liu, H. Cui, J. Li, M. Chen, A research on the cadmium ions adsorption of Sulfhydryl- And sulfo-functionalized UIO-66 with silica layer from water, J. Environ. Chem. Eng. 9 (2021), https://doi.org/10.1016/j.jece.2020.104621 104621.
[48] L. Fu, S. Wang, G. Lin, L. Zhang, Q. Liu, H. Zhou, C. Kang, S. Wan, H. Li, S. Wen, Post-modification of UiO-66-NH_2 by resorcyl aldehyde for selective removal of Pb(II) in aqueous media, J. Clean. Prod. 229 (2019) 470–479, https://doi.org/10.1016/j.jclepro.2019.05.043.
[49] E. Darezereshki, A.K. Darban, M. Abdollahy, A. Jamshidi-Zanjani, Influence of heavy metals on the adsorption of arsenate by magnetite nanoparticles: Kinetics and thermodynamic, Environ. Nanotechnol. Monit. Manag. 10 (2018) 51–62.
[50] J. Saiz, E. Bringas, I. Ortiz, New functionalized magnetic materials for As^{5+} removal: Adsorbent regeneration and reuse, Ind. Eng. Chem. Res. 53 (2014) 18928–18934, https://doi.org/10.1021/ie500912k.
[51] O. Mangla, S. Roy, Monoclinic zirconium oxide nanostructures having tunable band gap synthesized under extremely non-equilibrium plasma conditions, Proceedings 3 (2018) 10, https://doi.org/10.3390/iocn_2018-1-05486.